Contributions to Geophysics and Geodesy Vol. 45/1, 2015 (53–65)

Modeling of CME and CIR driven geomagnetic storms by means of artificial neural networks

Miloš REVALLO[1], Fridrich VALACH[2], Pavel HEJDA[3], Josef BOCHNÍČEK[3]

[1] Earth Science Institute of the Slovak Academy of Sciences
Dúbravská cesta 9, 840 05 Bratislava, Slovak Republic; e-mail: geofmire@savba.sk

[2] Geomagnetic Observatory, Earth Science Institute of the Slovak Academy of Sciences
Komárňanská 108, 947 01 Hurbanovo, Slovak Republic; e-mail: fridrich@geomag.sk

[3] Institute of Geophysics, Academy of Sciences of the Czech Republic
Boční II/1401, 141 31 Prague 4, Czech Republic; e-mail: ph@ig.cas.cz, jboch@ig.cas.cz

Abstract: A model of geomagnetic storms based on the method of artificial neural networks (ANN) combined with an analytical approach is presented in the paper. Two classes of geomagnetic storms, caused by coronal mass ejections (CMEs) and those caused by corotating interaction regions (CIRs), of medium and week intensity are subject to study. As the model input, the hourly solar wind parameters measured by the ACE satellite at the libration point L1 are used. The time series of the Dst index is obtained as the model output. The simulated Dst index series is compared with the corresponding observatory data. The model reliabilty is assessed using the skill scores, namely the correlation coefficient CC and the prediction efficiency PE. The results show that the model performance is better for the CME driven storms than for the CIR driven storms. At the same time, it appears that in the case of medium and weak storms the model performance is worse than in the case of intense storms.

Key words: space weather, coronal mass ejections (CMEs), corotating interaction regions (CIRs), geomagnetic storms, magnetosphere, Dst index

1. Introduction

Space weather is a branch of space physics concerned with the conditions within the solar system which are driven by variable solar activity. The near-Earth space environment is influenced especially by the properties of the solar wind plasma and the frozen-in interplanetary magnetic field (IMF).

doi: 10.1515/congeo-2015-0013

Adverse space weather can influence the performance and reliability of technological equipment in space and on the Earth's surface. Methods for forecasting space weather have thus generated considerable research interest.

For the ground-based applications, the geomagnetic activity is the key manifestation of space weather. From the terrestrial perspective, space weather is associated especially with the Earth's magnetosphere (*Pulkkinen, 2007*). The processes in the magnetosphere have their consequences in the ionosphere and in the variations of the geomagnetic field, which can be observed at ground-based magnetic observatories. The causal connection between the solar activity and the geomagnetic activity has been reproved many times. Many phenomena of this causal chain have been understood in detail; however, reliable methods for forecasting magnetic storms still remain difficult to reach. Variety of models have been proposed to forecast geomagnetic activity; see e.g. *Rastätter et al. (2013)* for some model statistics and ranking.

In this study, we focus our interest on the geoeffectiveness of the solar energetic events, namely coronal mass ejections and corotating interaction regions, as the principal causers and drivers of geomagnetic storms. *Coronal mass ejections* (CMEs) are believed to be the primary cause of the largest and most damaging space weather disturbances. CMEs are expulsions of large quantities of plasma and magnetic field from the Sun's corona. The occurence rate of CMEs increases during the maximum of the solar activity cycle (*Kim et al., 2005*). *Corotating interaction regions* (CIRs) are associated with regions of open magnetic fields known as coronal holes where high speed solar wind can stream out. They are stable formations that can survive over several solar rotations. CIRs are believed to be an interplanetary origin of geomagnetic activity during the declining phase of the solar activity cycle (*Richardson et al., 2000*).

Apart from the CMEs and CIRs solar origins, in what follows we consider both events as they manifest themselves as the solar wind disturbances at the libration point L1. CMEs at the libration point L1 can be recognized by sharp increase of particles density and speed. As magnetic field lines are frozen in the plasmoid, the temperature is decreasing and the IMF oscillates on timescale of days. The time distribution of geomagnetic disturbances according to their cause and intensity shows large variability in the course of solar cycle. CIRs are typically manifested by short increase of particle

density and long (several days) increase of temperature and speed of the solar wind at the libration point L1. CIRs between fast and slow solar wind can thus periodically pass over the Earth and cause recurrent geomagnetic storms.

Numerous studies show that CME and CIR events are different with characteristics specific to their type. The events due to CME tend to be shorter, more intense, with higher solar wind speeds. CMEs are responsible for greater changes in geomagnetic response and have very high values for energy input to geomagnetic storms. CIRs may not be as intense in their onset, but they are more efficient in their energy transfer to the magnetosphere. Within CIRs, the IMF presents a highly fluctuating southward component (*Turner et al., 2006*) and thus the geoeffectiveness of CIRs is usually weaker than those of CMEs. In *Alves et al. (2006)*, the geoeffectiveness of CIRs was assessed during the solar wind observational period 1964–2003 and approximately one third of the CIR events observed near the Earth was found geoeffective. The contribution of CIRs and CMEs to geomagnetic activity during the 23rd solar cycle was assessed in *Zhang et al. (2008)*.

One of the most pronounced differences between CME and CIR driven geomagnetic storms is in their recovery phases (*Laughlin et al., 2008*). With a CME event, at the beginning of the recovery phase, the influx of high energy particles and ions from the ring current to the Earth's magnetosphere is cut off as particles decay and return to more stable values. With a CIR event, the recovery process tends to be a more continuous and drawn-out process as new particles are still being injected into the ring current during recovery (*Tsurutani et al., 2006*).

In our previous study *Revallo et al. (2014)*, we attempted to set up a short-term (1 hour) prediction model for intense geomagnetic storms of the 23rd solar cycle. The model was fed with the solar wind parameters registered by the ACE satellite operating at the libration point L1. Here, the model is revisited and supplied with entries corresponding to the CME and CIR events resulting into geomagnetic storms of medium and low intensities. Besides of strong geomagnetic storms those of low intensities are of interest as well. For example, when performing magnetic surveys there is need for reliable forecast of any geomagnetic disturbances.

The underlying study deals with two principal questions: (1) Is the model

developed and tested for intense geomagnetic storms in *Revallo et al. (2014)* also usable for geomagnetic storms of medium and low intensities? (2) How is the model reliability for CME and CIR driven storms and can the model distinguish between these two types of storms?

To this end, the data sources and data selection criteria need to be specified first in Section 2. In Section 3 the mathematical model is described, results are presented in the form of graphs and comparison with observations and evaluation of skill scores is performed. Finally in Section 4 the main findings are summarized.

2. Data used

The data selection is motivated by the survey concerning different geomagnetic storm drivers of *Cramer et al. (2013)*. We collect 16 geomagnetic storms with previously identified drivers (CMEs and CIRs) with medium and low intensities recorded during the period of 1995–2005, as shown in Table 1.

The Dst index is used throughout the analysis to quantify the geomagnetic response. Here, we restrict ourselves to medium and weak geomagnetic storms with $Dst_{min} > -200\,\mathrm{nT}$. This selection is complementary to the choice of intense geomagnetic storms in *Revallo et al. (2014)*. The final values of the Dst index are provided by the Kyoto WDC.

At the model input, we supply the solar wind parameters measured by the ACE satellite operating at the libration L1 point and provided by the OMNIWeb database at `http://omniweb.gsfc.nasa.gov`. The hourly mean solar wind data needed to feed the model are the bulk speed, the proton density, the kinetic proton temperature and the z component of the IMF.

3. Model and results

Here we adopt the model which was developed in *Revallo et al. (2014)* combining *the method of artificial neural networks* (ANN) and the analytical approach known from *Romashets et al. (2008)*. The whole model development is not reproduced here, instead we refer to *Romashets et al. (2008)* and *Revallo et al. (2014)* for computational details.

Table 1. A list of CME and CIR driven geomagnetic storms according to Table 1 in *Cramer et al. (2013)*. The final values of Dst_{min} are shown, according to the Kyoto WDC. The values of the correlation coefficient CC and the prediction efficiency PE are defined by (8) and (9) in Section 3.3.

Event	Date	Driver	$Dst_{min}[nT]$	CC	PE
Apr 1995	07/04/1995	CIR	-149	0.40	0.16
Aug 1995	22/08/1995	CME	-61	0.89	0.67
May 1997	15/05/1997	CME	-115	0.64	0.38
Mar 1998	10/03/1998	CIR	-116	0.47	0.21
Jun 1998	06/06/1998	CIR	-50	0.54	0.27
Aug 1998	06/08/1998	CME	-138	0.57	0.25
Nov 1998	08/11/1998	CME	-149	0.90	0.55
Jan 2000	11/01/2000	CIR	-81	0.49	0.24
Feb 2000	11/02/2000	CME	-133	0.58	0.33
Oct 2000	28/10/2000	CME	-127	0.84	0.67
Nov 2002	20/11/2002	CIR	-128	0.40	0.07
Jul 2003	10/07/2003	CIR	-105	0.25	-0.15
Oct 2003	13/10/2003	CIR	-85	0.20	-0.11
May 2005	07/05/2005	CIR	-110	0.34	0.08
Aug 2005	10/08/2005	CME	-47	0.70	0.49
Oct 2005	31/10/2005	CME	-74	0.83	0.66

3.1. Mathematical model

The model of interaction between the solar wind and magnetosphere proposed by *Romashets et al. (2008)* allows for analytical computation of *the jump in magnetic field* $[B_t]$ when moving from the solar wind (the external field) to the magnetosphere (the internal field). The function $[B_t]$ has been pointed out to play crucial role in geomagnetic response evaluation in terms of the Dst index.

The magnitude of the jump $[B_t]$ across the magnetopause depends on the solar wind parameters (*Romashets et al., 2008*) as follows

$$[B_t] = B_z \left[4.2629 \left(\frac{V_\infty}{500} \right) \left(\frac{10^6}{T_\infty} \right)^{1/2} - 1 \right] - 34.2109 \left(\frac{n_\infty}{5} \right)^{1/2} \left(\frac{V_\infty}{500} \right) . \quad (1)$$

Here, the subscript $_\infty$ stands for the undisturbed solar wind fields far before the interaction with the magnetosphere; V_∞ is the velocity measured in $\mathrm{km\,s^{-1}}$, n_∞ is the particle density measured in $\mathrm{cm^{-3}}$, T_∞ is the temperature measured in K and B_z represents the z component of the IMF measured in nT.

In (1), the hourly means of the solar wind data are used to compute the function $[B_t]$ and therefore the notation $[B_t]_k$ is adopted hereafter for its discrete values. To take account for the IMF orientation, similarly as in *Revallo et al. (2014)* we define *the entry functions* x_k by

$$x_k = \frac{1}{2}[1 - sgn(B_{zk})][B_t]_k \,. \tag{2}$$

Geomagnetic response measured by the Dst index is proportional to a weighted sum of the hourly contributions of x_k.

3.2. Application of artificial neural networks

To determine the weights measuring the importance of the entry functions x_k, we have proposed the method of ANN; for details see *Revallo et al. (2014)*. The ANN has been designed to consist of 13 input neurons for the entries x_k ($k = 0$ to 12) and 1 output neuron. The ANN has been trained to produce the model Dst^n index. Note that in *Revallo et al. (2010)*, the original empirical model known from *Romashets et al. (2008)* was treated with the hourly steps N as a free parameter. Varying N, the model Dst^n index series was produced in order to minimize the normalized mean square error.

In what follows, we adopt the ANN model with the hourly steps fixed at $N = 12$ as in *Revallo et al. (2014)*. To determine the values of the weighting functions, the preliminary ANN model has been set up first in *Revallo et al. (2014)* Section 3.3. Consequently, more sophisticated ANN model possesing hidden layer of neurons has been designed to produce the model values of the Dst^n index. We have shown exactly, the ANNs possessing low number of hidden neurons to provide best results (see Figs. 2,3 in *Revallo et al. (2014)*). For the model Dst^n index calculation, we could thus restrict ourselves to ANNs possessing simpler architecture.

In this study, we compute the model Dst^n index using the ANN without hidden layer of neurons. The output function Out can be expressed as

$$Out = f\left(\sum_{k=0}^{12} w_k In_k - \Theta\right) \tag{3}$$

where f is the logistic regression function

$$f(z) = \frac{1}{1+\exp(-z)} \tag{4}$$

In_k ($k = 0$ to 12) is the input vector and w_k ($k = 0$ to 12) is the vector of weights. Function Θ characterizes the sensitivity threshold of the output neuron. The values of w_k ($k = 0$ to 12) and Θ are adopted from *Revallo et al. (2014)*.

Similarly as in *Revallo et al. (2014)*, we rescale the input In_k and output Out of the ANN model for computational convenience and relate with the entry functions x_k and the model Dst^n index as follows

$$In_k = \frac{x_k + 248.4}{1417} \qquad k = 0 \text{ to } 12\,, \tag{5}$$

$$Dst^n = \xi\,\frac{Out - 0.896}{0.002}\,. \tag{6}$$

In addition to the fixed re-scaling parameters in (5) and (6), the free parameter ξ is introduced to minimize the normalized mean square error $NMSE$ defined by

$$NMSE = \frac{1}{M^2}\sum_{s=1}^{M}\left[Dst_s^n - Dst_s\right]^2 \tag{7}$$

where M is the length of the record (in hours).

The observed Dst index series and the model Dst^n index series for the geomagnetic storms considered are shown in Figs. 1a,b.

3.3. Comparison with observations

In order to assess the agreement between the computed Dst^n index and the observational Dst index, we adopt the skill scores: the correlation coefficient CC and the prediction efficiency PE, similarly as in *Rastätter et al. (2013)*.

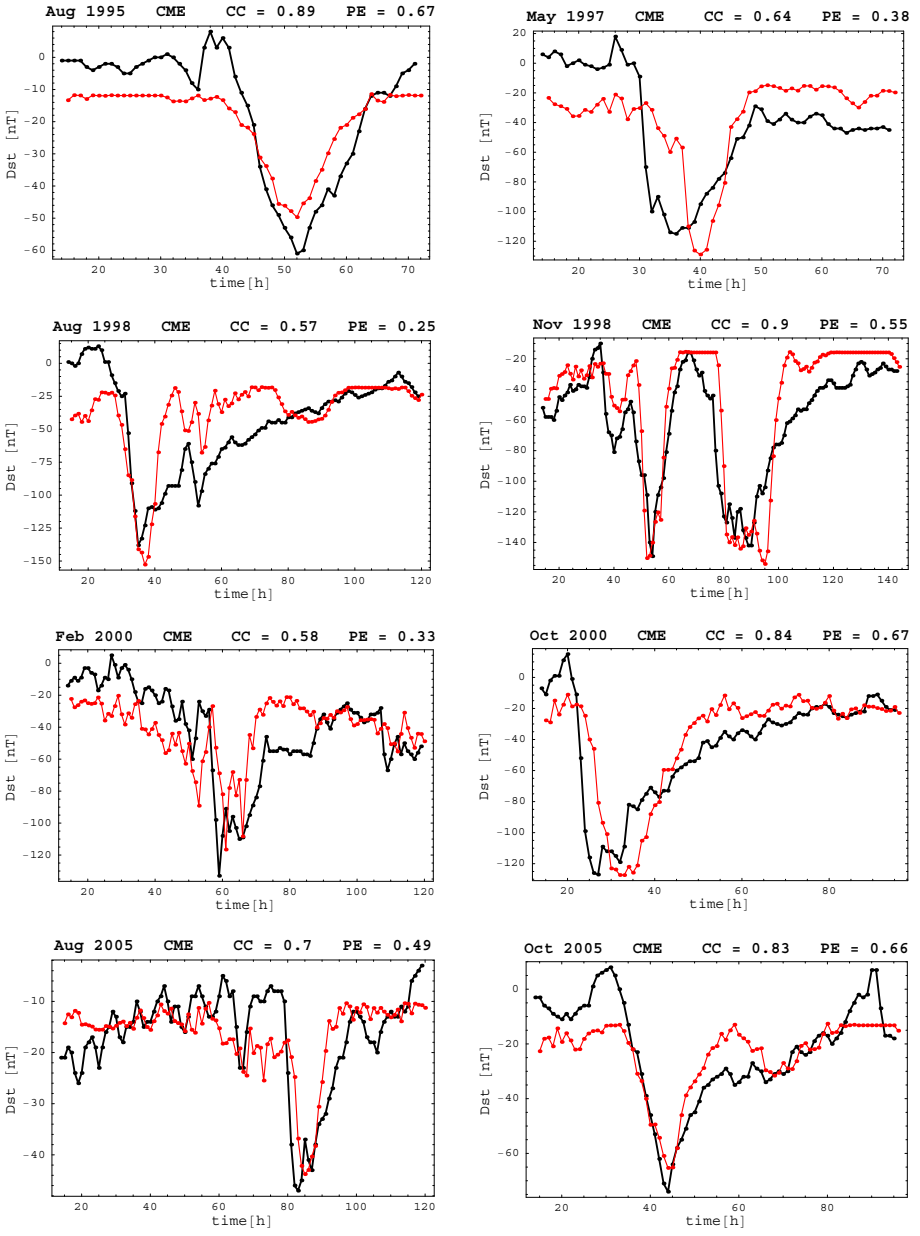

Fig. 1a. The observational *Dst* index series (black line) and the model Dst^n index series (red line) for 8 CME driven geomagnetic storms shown in Table 1.

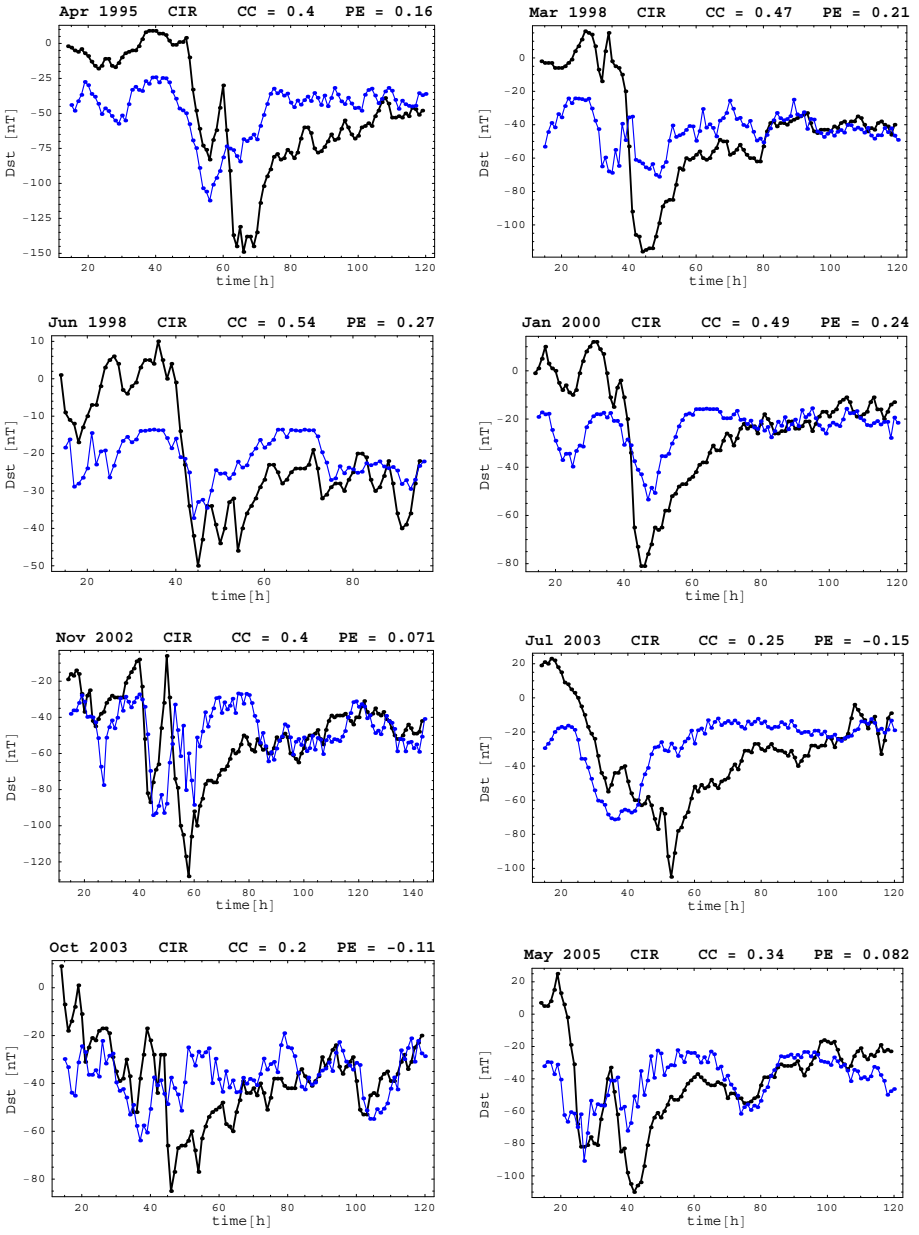

Fig. 1b. The observational *Dst* index series (black line) and the model Dst^nindex series (blue line) for 8 CIR driven geomagnetic storms shown in Table 1.

The correlation coefficient CC between the series of Dst^n and Dst is defined as

$$CC = \frac{\sum_{s=1}^{M}(Dst_s - \overline{Dst})(Dst_s^n - \overline{Dst^n})}{\sqrt{\sum_{s=1}^{M}(Dst_s - \overline{Dst})^2}\sqrt{\sum_{s=1}^{M}(Dst_s^n - \overline{Dst^n})^2}} \tag{8}$$

where $\overline{Dst^n}$ and $\overline{Dst}$ stand for the arithmetic means of the series of Dst^n and Dst, respectively, and M is the length of the record. Using the same notation, *the prediction efficiency* PE for a discrete time series is defined as

$$PE = 1 - \frac{\sum_{s=1}^{M}(Dst_s - Dst_s^n)^2}{\sum_{s=1}^{M}(Dst_s - \overline{Dst})^2}\,. \tag{9}$$

The value $PE = 1$ indicates perfect model performance and $PE = 0$ indicates performance comparable to predicting the arithmetic mean of the observed signal. PE can reach unlimited negative values. The values $PE < 0$ occur when the observed mean is a better predictor than the model. In contrast to the correlation coefficient, PE includes the amplitude of the modeled signal in addition to the shape of the time series. Signals with good correlation but incorrect amplitudes may result in negative PE scores.

The skill scores for each particular event are shown in graphs in Figs. 1a,b and are also summarized in Table 1.

4. Discussion and conclusions

The purpose of the research done herein was to assess the contribution of CMEs and CIRs to geomagnetic activity of various intensity and to assess the reliability of the model developed in *Revallo et al. (2014)*.

Inspecting the graphs in Fig. 1 and the skill scores CC and PE in Table 1, it can be observed that the presented model performs best for the CME driven storms, i.e. those with more pronounced sudden storm commencements (SSC), deeper main phases and faster return phases. On the other hand, the model scores poorly for the CIR driven storms, i.e. those with slow return phases and complicated Dst index record. In general, for the medium and weak storms considered here, the skill scores CC and PE are smaller than those for the intense storms (Table 1 in *Revallo et*

al. (2014)). This behaviour is due to the fact, that the intense storms studied in *Revallo et al. (2014)* possess deep minima, which could be better captured by the presented model.

A variety of models for geomagnetic storms is known at present. For example, in Table 3 in *Rastätter et al. (2013)*, three classes of models were subject to ranking: the 3D magnetosphere models, the ring current kinetic models and the Dst-specification models. None of these models consistently performed best for all events and model ranking varied widely by skill score used. The presented model falls into the class of Dst-specification models, however exact comparison and inclusion to the ranking chart in *Rastätter et al. (2013)* is not possible, due to different choice of events and different lenghts of data records.

The presented model is based on an analytical model of the solar-wind magnetosphere interaction. We have proved such approach to be able to capture the essential features of a geomagnetic storm. However, there are other possible issues that might improve the models, especially those for CIR driven storms. For example, when evaluating the energy input to the magnetosphere the empirical energy function is used, known as the epsilon parameter ϵ (see e.g. *Turner et al. (2009)*) and defined by

$$\epsilon = \frac{4\pi}{\mu_0} v B^2 \sin^4\left(\frac{\theta}{2}\right) l_0^2 \,. \tag{10}$$

Here θ is the solar wind clock angle, l_0^2 is a characteristic length scale of the magnetosphere, μ_0 is the permeability of free space, v is the solar wind velocity and B is the total magnetic field. More extensive study of the energetics of the CME and CIR driven geomagnetic storms can contribute to understanding of their possible physical drivers and also help to improve forecasting methods.

At this stage we are able to answer the questions posed in Introduction: (1) The general observation is that in the case of medium and weak geomagnetic storms the model performance is worse than in the case of intense geomagnetic storms (compare with results in *Revallo et al. (2014)*). (2) Due to more complex Dst index record, the CIR driven storms are modelled with less accuracy that those driven by CMEs.

Acknowledgments. This work was supported in part by VEGA Grant 2/0030/14 of the Scientific Grant Agency of the Ministry of Education of Slovak Republic and the

Slovak Academy of Sciences and by the Slovak Research and Development Agency under the contract No. APVV-0662-12. The authors are grateful for constructive comments of the anonymous referees.

References

Alves M. V., Echer E., Gonzalez W. D., 2006: Geoeffectiveness of corotating interaction regions as measured by Dst index. J. Geophys. Res., **111**, A7, doi: 10.1029/2005JA011379.

Cramer W. D., Turner N. E., Fok M.-C., Buzulukova N. Y., 2013: Effects of different geomagnetic storm drivers on the ring current: CRCM results. J. Geophys. Res., **118**, 1062-1073, doi: 10.1002/jgra.50138.

Kim R.-S., Cho K.-S., Moon Y.-J., Kim Y.-H., Yi Y., Dryer M., Bong S.-C., Park Y.-D., 2005: Forecast evaluation of the coronal mass ejection (CME) geoeffectiveness using halo CMEs from 1997 to 2003. J. Geophys. Res., **110**, A11104, doi: 10.1029/2005JA011218.

Laughlin L. K., Turner N. E., Mitchell E. J., 2008: Geoeffectiveness of CIR and CME events: Factors contributing to their differences. Journal of the Southeastern Association for Research in Astronomy, **2**, 19–22.

Pulkkinen T., 2007: Space Weather: Terrestrial Perspective. Living Rev. Solar Phys., **4**, 1, URL (cited on 24/01/2014): `http://www.livingreviews.org/lrsp-2007-1`, doi: 10.12942/lrsp-2007-1.

Rastätter L., Kuznetsova M. M., Glocer A., Welling D., Meng X., Raeder J., Wiltberger M., Jordanova V. K., Yu Y., Zaharia S., Weigel R. S., Sazykin S., Boynton R., Wei H., Eccles V., Horton W., Mays M. L., Gannon J., 2013: Geospace environment modeling 2008-2009 challenge: Dst index. Space Weather, **11**, 187–205, doi: 10.1002/swe.20036.

Revallo M., Valach F., Hejda P., Bochníček J., 2014: A neural network *Dst*-index model driven by input time histories of the solar wind-magnetosphere interaction. Journal of Atmospheric and Solar Terrestrial Physics, **110–111**, 9–14, doi: 10.1016/j.jastp.2014.01.011.

Revallo M., Valach F., Váczyová M., 2010: The geomagnetic storm of August 2010 as a lesson of the space weather modelling. Contributions to Geophysics and Geodesy, **40**, 4, 313–322, doi: 10.2478/v10126-010-0013-5.

Richardson I. G., Cliver E. W., Cane H. V., 2000: Sources of geomagnetic activity over the solar cycle: Relative importance of coronal mass ejections, high-speed streams, and slow solar wind. J. Geophys. Res., **105**, A8, 18203–18213, doi: 10.1029/1999JA000400.

Romashets E. P., Poedts S., Vandas M., 2008: Modeling of the magnetic field in the magnetosheath region. J. Geophys. Res., **113**, A02203, doi: 10.1029/2006JA012072.

Tsurutani B. T., Gopalswamy N., McPherron R. L., Gonzalez W. D., Lu G., Guarnieri F. L., 2006: Magnetic storms cause by corotating solar wind streams. In: Recurrent Magnetic Storms: Corotating Solar Wind Streams, Edited by Tsurutani B., McPherron R.,. Gonzalez W. D, Lu G., Sobral J. H. A., Gopalswamy N., 1–18.

Turner N. E., Cramer W. D., Earles S. K., Emery B. A., 2009: Geofficiency and energy partitioning in CIR-driven and CME-driven storms. Journal of Atmospheric and Solar Terrestrial Physics, **71**, 10-11, 1023–1031, doi: 10.1016/j.jastp.2009.02.005.

Turner N. E., Mitchell E. J., Knipp D. J., Emery B. A., 2006: Energetics of magnetic storms driven by corotating interaction regions: A study of geoeffectiveness. In: Recurrent Magnetic Storms: Corotating Solar Wind Streams, Edited by Tsurutani B., McPherron R., Gonzalez W. D., Lu G., Sobral J. H. A., Gopalswamy N., 113–124.

Zhang Y., Sun W., Feng X. S., Deehr C. S., Fry C. D., Dryer M., 2008: Statistical analysis of corotating interaction regions and their geoeffectiveness during solar cycle 23. J. Geophys. Res., **113**, A8, doi 10.1029/2008JA013095.